THE JOURNAL OF PHYSICAL CHEMISTRY C

Article

pubs.acs.org/JPCC

Bonding and Charge Transfer in Metal–Organic Coordination Networks on Au(111) with Strong Acceptor Molecules

Marisa N. Faraggi,[†,#] Nan Jiang,[‡,#] Nora Gonzalez-Lakunza,[†] Alexander Langner,[‡] Sebastian Stepanow,*[,‡] Klaus Kern,[‡,§] and Andres Arnau*[,‡,∥,⊥]

[†]Donostia International Physics Center DIPC, P. Manuel de Lardizabal 4, 20018 San Sebastián, Spain

[‡]Max-Planck-Institut für Festkörperforschung, D-70569 Stuttgart, Germany

[§]Institut de Physique de la Matière Condensée, École Polytechnique Fédérale de Lausanne, CH-1015 Lausanne, Switzerland

[∥]Centro de Física de Materiales CFM-MPC, Centro Mixto (CSIC-UPV/EHU), San Sebastián, Spain

[⊥]Departamento de Física de Materiales, Facultad de Química UPV/EHU, San Sebastián, Spain

Supporting Information

ABSTRACT: The geometric and electronic structure of two structurally similar metal–organic networks grown on the Au(111) surface is investigated by scanning tunnelling microscopy (STM) and spectroscopy (STS) combined with density functional theory (DFT) calculations. The networks are composed of (i) F4TCNQ ($C_{12}F_4N_4$, 2,3,5,6-tetrafluoro-7,7,8,8-tetracyanoquino–dimethane) molecules and Au adatoms segregated from the pristine metal surface, and (ii) TCNQ ($C_{12}H_4N_4$, 7,7,8,8-tetracyanoquinodimethane) and codeposited Mn atoms. In both cases, the strong electron acceptor character of the molecules results in metal–to-ligand charge transfer to the lowest unoccupied molecular orbital (LUMO). The amount of electrons donated from the 4-fold coordinated Mn atoms to TCNQ is higher compared to the 2-fold coordinated Au adatoms to F4TCNQ. This behavior is reflected in the appearance of distinct spectral features in STS data in the energy region close to the Fermi level resulting from the intricate interplay between surface states, adatom states, and molecular orbitals. These observations are consistent with a picture in which the LUMO of the TCNQ acceptor molecule hybridizes with Mn and Au substrate metal states becoming practically filled, while the LUMO of F4TCNQ is only partially filled despite being the stronger electron acceptor. Our results reveal the importance of the type of bonding between the strong acceptor and the metal center (Au or Mn) as well as its coordination in the determination of the charge transfer to the adlayer, which is important for its electronic properties.

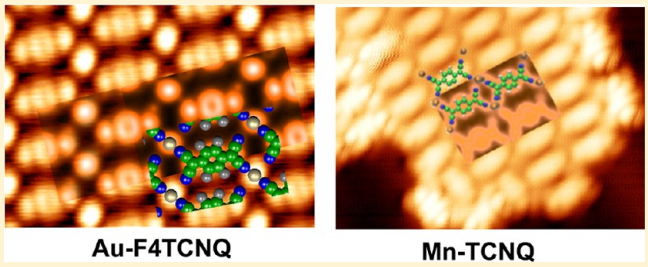

INTRODUCTION

The formation of two-dimensional (2D) metal–organic coordination networks on surfaces comprising organic ligands and metal centers has recently become a subject of active research interest due to its potential applications in different fields ranging from surface patterning, heterogeneous catalysis, magnetism and host–guest chemistry.[1−10] The synthesis and growth of particular networks and coordination structures depend on the relative strength of the interactions between the constituents and with the underlying substrate. This latter can play an important role in the growth of the overlayer structure because, occasionally, it may provide native adatoms from the pristine metal surface as metal coordination centers[11−13] or even induce surface reconstructions[14] when it is strong. In particular, the herringbone reconstruction of the close packed Au(111) surface can be modified to a major or lesser extent depending on the strength of the adsorbate–substrate coupling.[15−19] Indeed, the chemical state of the organic ligands and metal centers can be significantly modified due to vertical charge transfer from the surface. In addition, lateral charge transfer between the constituents is crucial for the bonding and equally important for the electronic and chemical properties of the adlayers. The metal centers play an active role in the formation of the two-dimensional arrays by favoring particular coordination numbers and modes that result in a given stoichiometry determining the charge and magnetic moment of both the metal center and organic ligand. Eventually, this could be used to control the electronic and magnetic properties of the interface.[20,21]

Strong electron acceptors, like TCNE (C_6N_4, tetracyanoethylene), TCNQ ($C_{12}H_4N_4$, 7,7,8,8-tetracyanoquinodimethane) or F4TCNQ ($C_{12}F_4N_4$, 2,3,5,6-tetrafluoro-7,7,8,8-tetracyanoquinodimethane), have been shown to be efficient in controlling the electron charge transfer at the metal–organic interface[14,22−24] and, thus, permit the reduction of the energy barriers for the injection of holes by a proper work function

Received: July 9, 2012
Revised: October 31, 2012
Published: October 31, 2012

   dx.doi.org/10.1021/jp306780n | J. Phys. Chem. C 2012, 116, 24558–24565

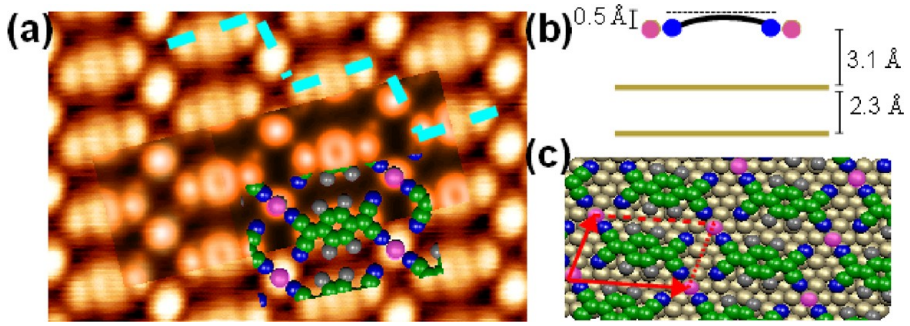

Figure 1. (a) High-resolution STM image (5 nm × 3 nm) of Au−F4TCNQ network structures assembled on Au(111) (I = 0.2 nA and U = 89 mV) with STM simulated image superposed. The dashed blue lines guide the eye to identify the zig−zag coordination chains formed by Au adatoms and F4TCNQ. (b) Side view representation showing the bending of F4TCNQ that amounts almost 0.5 Å, the vertical displacement of the highest C atom in the central ring of the molecule with respect to the Au adatom metal center. (c) Optimized structural model based on STM data. The unit cell lattice vectors are indicated by red arrows. C, N, and F atoms are represented by green, blue, and dark gray circles, respectively. The pink circles between F4TCNQ molecules represent Au adatoms which are coordinated with two CN groups only.

change. Additional coordination with transition metal atoms[25,26,45] that have a magnetic moment, like Fe, Co, Ni, or Mn, is expected to permit the localization of spins in the 2D metal−organic network and, therefore, represent an interesting challenge for the design and fabrication of nanoscale devices. The type and strength of magnetic coupling (ferromagnetic and antiferromagnetic) between the metal centers is mediated by the electron accepting ligands. The coordination structure, stoichiometry, and resulting charge state of the ligands are crucial for the determination of the magnetic properties. Thus, high-resolution scanning tunnelling spectroscopy (STS) in combination with first principles calculations can be the ideal tools to obtain valuable insight into these issues for the 2D analogue metal−organic coordination networks self-assembled on an inert support.

In this work, we study two different systems forming similar supramolecular coordination networks on the Au(111) surface. The first network is obtained by evaporation of F4TCNQ molecules onto the metal surface, and the second structure consists of TCNQ molecules and codeposited Mn atoms. In both cases, well-ordered quasi-rectangular superstructures are formed. These are characterized by low-temperature high-resolution scanning tunnelling microscopy as well as dI/dV spectroscopy, combined with density functional theory calculations for the interpretation of the observations. Our basic findings can be summarized as follows: (i) F4TCNQ molecules are 2-fold coordinated with native Au adatoms segregated from the pristine Au(111) surface at room temperature; (ii) the Mn coordination centers are 4-fold coordinated to the TCNQ ligands; (iii) the degree of electron charge transfer from the Mn atoms to the TCNQ molecule is higher compared to that from the Au adatoms to F4TCNQ and, thus, reflects the differences in F4TCNQ−Au and TCNQ−Mn bonding; (iv) the calculated electronic structure close to the Fermi level for both systems shows specific characteristics that are consistent with the observed features in scanning tunnelling spectroscopy.

METHODS

The experiments were carried out in an ultrahigh vacuum chamber with a base pressure better than 2×10^{-10} mbar in the preparation chamber and lower than 1×10^{-11} mbar in the STM. The Au(111) surface was cleaned by repeated cycles of Ar^+ sputtering and subsequent annealing to 800 K. Both ligands, TCNQ (98%, Aldrich) and F4TCNQ (97%, Aldrich), were deposited by organic molecular-beam epitaxy (OMBE) from a resistively heated quartz crucible at a sublimation temperature of 408 K onto the clean Au(111) surface kept at room temperature. The coverage of molecules was controlled to be below one monolayer. After the deposition of F4TCNQ no further annealing was carried out. Mn was subsequently deposited by an electron-beam heating evaporator at a flux of 0.01 monolayer/min on top of the TCNQ adlayer held at 350 K. We find no dependence on the Mn:TCNQ ratio in the formation of the overlayer structure. The substrate was subsequently transferred to the low-temperature STM and cooled to 5 K. STM images were acquired with typical parameters of 0.1−1 nA and ±0.5−1.2 V. The dI/dV spectra were acquired using a lock-in amplifier modulating the bias voltage at a frequency of 2.55 kHz above the cutoff frequency of the feedback loop with an amplitude V_{rms} = 10 mV. To obtain information on the lateral extension of the resonances, dI/dV maps at a fixed bias voltage were acquired in the constant current mode (feedback loop closed).

DFT calculations were done using the Vienna Ab Initio Simulation Package (VASP).[27,28] The Au(111) surface was modeled using a periodic supercell made of four Au atomic planes and additional vacuum equivalent to four atomic layers in the $\hat{z}$ direction (~13 Å), large enough to avoid residual interactions due to supercell periodic boundary conditions. The ion-electron interactions were described with the Projector Augmented-Wave (PAW) method,[29] and the Generalized Gradient Approximation (GGA) was used for exchange and correlation.[30] We used a kinetic energy cutoff of 280 eV in the plane wave expansion and an electronic convergence criterion of 10^{-5} eV for the energy value. The summations in the surface Brillouin zone were done using a k-point sampling equivalent to more than 10 × 10 k-points in the 1 × 1 surface unit cell of Au(111). A relaxation of atomic positions was performed assuming a convergence criterion of 0.2 eV/Å. Once the optimized structure is obtained from the standard energy minimization procedure, the electronic structure is calculated. In the case of the metal−organic coordination network formed by Mn atoms and TCNQ we do spin polarized calculations using the DFT+U approach[31] for the Mn d-electrons with U = 4 eV. This value of U = 4 eV gives the correct energy splitting of the 3d majority and minority Mn bands and is close the value U = 4.2 eV used by Tseng *et al.* in a similar study of Mn−TCNQ on Cu(100).[25,45] Concerning the STM simulations, we

dx.doi.org/10.1021/jp306780n | J. Phys. Chem. C 2012, 116, 24558−24565

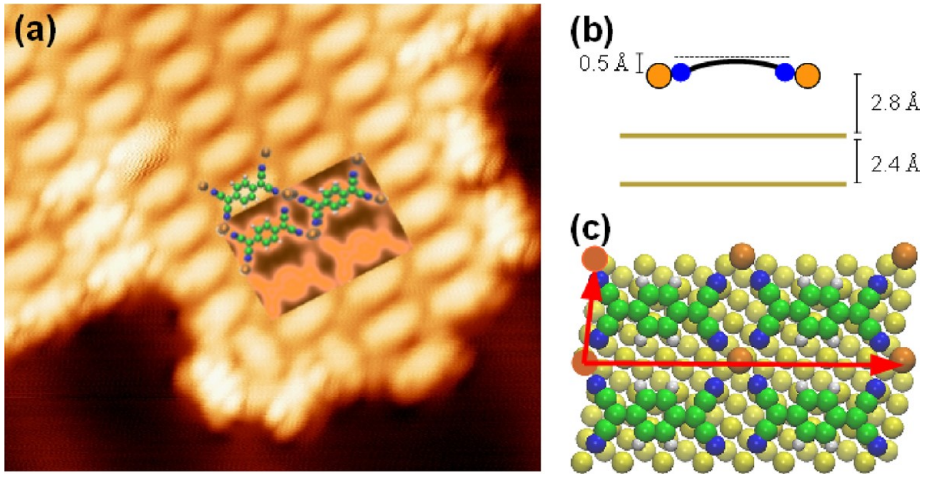

Figure 2. (a) Experimental STM image (8 nm × 6.6 nm) of Mn−TCNQ on Au(111) (I = 0.17 nA and U = +1.2 V) with an schematic geometrical representation. The STM simulated image is superposed. (b) Side view of the Mn−TCNQ/Au(111) structural model with distances in Å. It shows a similar bending as Au−F4TCNQ/Au(111) in Figure 1b. (c) Optimized structural model based on STM data (unit cell vectors are drawn in red). C, N and H atoms are represented by green, blue, and light gray circles, respectively. The golden circles between TCNQ molecules represent Mn atoms which are coordinated with four CN groups.

have used the energy integrated local density of states ILDOS(x,y,z) with an energy window defined by the applied bias voltage following the Tersoff-Hamann approach[32] to produce constant height STM images ILDOS(x,y,z_c) with a vertical displacement z_c = 2.5 Å, measured from the metal atom (Au or Mn) position. These STM simulations show the same qualitative (x,y) spatial variation as the constant current z(x,y) STM images but its range of variation is larger (almost exponential in ILDOS) compared with the constant current STM topographies (basically linear in z). Therefore, a direct quantitative comparison is not done.

RESULTS AND DISCUSSION

Figures 1a and 2a show high resolution STM images of the F4TCNQ and Mn−TCNQ metal−organic networks, respectively. At a first glance, the STM topographical images show similar well-ordered domains of F4TCNQ and TCNQ molecules in which the appearance of both molecules resembles the shape of the LUMO.[35,36] In particular the under-coordinated TCNQ molecules, that is, coordinating to less than 3 Mn atoms, located at the domain perimeter clearly show the LUMO structure (see also Supporting Information (SI), Figure S3). The elongated shape of the molecules are aligned within the quasi-rectangular pattern of the domains. A closer inspection reveals two important differences between the structures: (i) in Figure 1 there are bright and nearly circular protrusions within the adlayer connecting apparently two F4TCNQ molecules, while in Figure 2 only the TCNQ molecules are clearly resolved, and (ii) the Mn−TCNQ superstructure exhibits a nearly perfect rectangular lattice, whereas the F4TCNQ adlayer has a clear rhomboidal distortion. Additionally, the Au(111) herringbone reconstruction remains unaffected by the Mn−TCNQ domains, but vanishes underneath the F4TCNQ superstructure (SI, Figures S1 and S2).

As shown below, on the basis of first principles calculations and the complementary information contained in the STS data (Figures 3 and 4), we assign the bright and spherical features in the F4TCNQ domains to Au adatoms segregated from the pristine Au(111) surface. This results in the observed lifting of

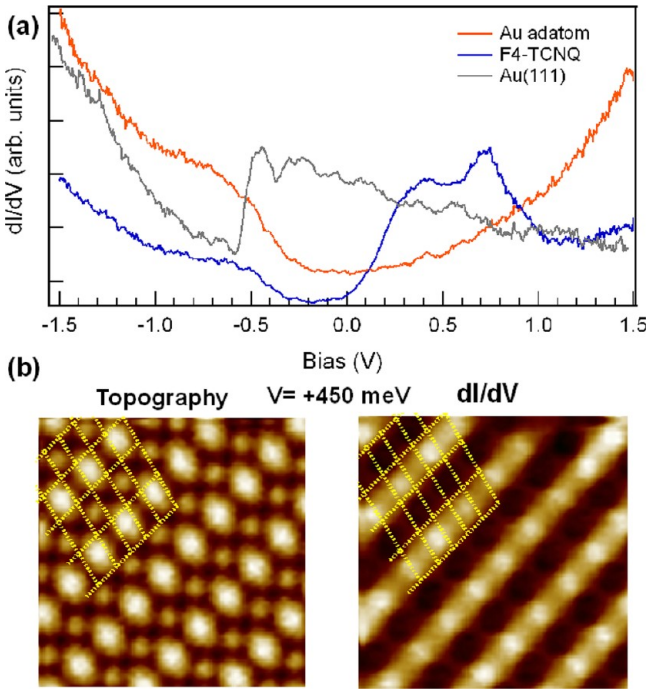

Figure 3. System F4TCNQ on Au(111): (a) STS measurements taken on different spots of the island; (b) set of topographic image and dI/dV map (5 nm × 5 nm, I = 0.5 nA) taken at V = +450 mV with a superposed yellow grid showing the different contrast in the two images.

the herringbone reconstruction below the F4TCNQ domains. The resulting structure is commensurate with the Au surface registry while the rectangular Mn−TCNQ structure exhibits a larger apparent unit cell (cf. Figure 2c). This dissimilarity is reflected in the different domain sizes obtained for both structures (SI, Figures S1 and S2). The Au−F4TCNQ domains can cover entire substrate terraces, whereas the Mn−TCNQ domains rarely exceed 25 nm in size. As F4TCNQ is a stronger acceptor than TCNQ, it induces a rearrangement of charge in the system that includes both Au(111) and F4TCNQ electrons, while TCNQ does not seem to affect the Au(111) surface. The

dx.doi.org/10.1021/jp306780n | J. Phys. Chem. C 2012, 116, 24558−24565

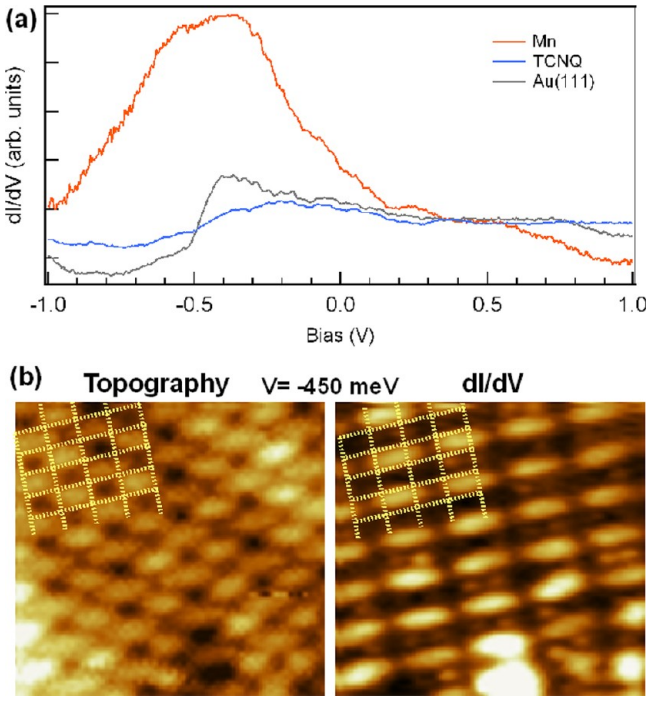

Figure 4. System Mn−TCNQ on Au(111): (a) similar to Figure 3a; (b) set of topographic image and dI/dV map (5 nm × 5 nm, I = 0.5 nA) taken at V = −450 mV with a superposed yellow grid showing the different contrast in the two images.

charge donation from the metal surface to the F4TCNQ induces the segregation of Au atoms from the herringbone reconstruction, similar to the case of strong electronegative atom adsorption.[33,34]

The optimal geometry and corresponding electronic structure of the metal−organic adlayers were calculated using the density functional theory (DFT) based code implemented in VASP. Commensurate overlayers were enforced due to the periodic supercell approach. As an initial guess for the structures approximate lattice parameters obtained from the STM images were used. In the case of F4TCNQ, calculations with and without additional Au adatoms at the position of the spherical protrusions were carried out. The DFT results strongly support the structure with Au adatoms, based on both the energetic analysis and the STM simulations. The STM simulation of the Au−F4TCNQ structure superposed to the STM data in Figure 1a shows excellent agreement. Figure 1c shows the resulting surface unit cell of the superstructure indicated by red arrows. The corresponding lattice vectors (b_1) and (b_2) are $\begin{pmatrix} b_1 \\ b_2 \end{pmatrix} = \begin{pmatrix} 5 & 2 \\ 1 & 3 \end{pmatrix} \begin{pmatrix} a_1 \\ a_2 \end{pmatrix}$, where (a_1) and (a_2) are the Au(111) surface unit vectors. The pink circles between F4TCNQ molecules represent Au adatoms which are coordinated with two CN groups only. This N−Au adatom bond length amounts to 1.96 Å, while the other two CN groups pointing to the Au adatom are at a N−Au distance of more than 3.4 Å. For the Mn−TCNQ structure a unit cell containing two Mn atoms and two TCNQ ligands had to be used to enforce a commensurate superstructure that is in agreement with the observed angles and distances obtained from the STM data as shown in Figure 2c. In this case the matrix describing the superstructure is $\begin{pmatrix} 9 & 2 \\ 1 & 3 \end{pmatrix}$. The simulated STM image is also superimposed to the STM data in Figure 2a. The agreement is rather good, in particular the missing bright contrast at the positions of the Mn coordination centers. In this structure each Mn center coordinates to four TCNQ ligands via the cyano groups, the N−Mn bond length being 2.3 Å.

The optimized molecular adsorption geometry for both systems presents a nonplanar ligand, in which the cyano groups are bent with respect to the aromatic rings (the N atoms are about 0.5 Å lower) to form bonds with the Au or Mn metal centers (see Figures 1b and 2b). In the case of F4TCNQ also the two cyano groups not bonded to Au adatoms are bent down, similar to the Mn-$(TCNQ)_2$ network formed on Cu(100).[25,45] This was ascribed to the electrostatic attraction between the N lone pairs and the positively charged metal surface atoms. This type of geometrical distortion, that is commonly observed for the anions, has also been found for TCNQ on Cu(100).[14]

In the following we discuss the electronic properties of the similar metal−organic adlayers, where the energy difference between the corresponding electron affinities of the molecules (F4TCNQ, TCNQ) and ionization potentials of the metal centers (Au, Mn) are comparable. This suggests that in the two systems with the same stoichiometry the coordination number (two or four) and type of chemical bond (more ionic or more covalent) with the metal centers is crucial in determining the charge state of the molecules. The different coordination is determined by the different Mn and Au adsorption sites that result from the different N−Au (1.9 Å) and N−Mn (2.3 Å) bond lengths. At this point it is worth recalling the differences in the Au/Mn atom valence electron structure with a completely/half filled 5d or 3d-shell and one/two outer 6s or 4s electrons, respectively. A first hint of the pronounced differences in the electronic structures can be seen already in the imaging at negative and positive bias voltages. In the Au−F4TCNQ system, both the Au adatoms and the TCNQ molecules are imaged as protrusions in the bias range from −1.5 to +1.5 V, while for Mn−TCNQ only the molecules are clearly resolved in the STM topographs. Only at high negative bias voltages the Mn atoms are seen with bright contrast (see Figure 4b).

The STS data for the Au−F4TCNQ and Mn−TCNQ networks are presented in Figures 3a and 4a, respectively. The dI/dV spectrum taken at the center of the F4TCNQ molecules present a broad (almost 1 eV) spectral feature with two maxima at +0.4 and +0.75 V that we assign tentatively to the LUMO, in agreement with previous observations.[24] However, we cannot discard that the LUMO and the Au(111) surface state hybridize giving rise to two new interface states of bonding and antibonding character. In any case, our data suggest a significant quenching of the pristine Au(111) surface state, whose characteristic fingerprint in STS is a step at about −0.5 V. For our F4TCNQ/Au(111) system under study, the dI/dV spectrum taken at the Au adatom position is rather structureless and does not present any spectral feature at positive bias voltages. The differential conductance becomes appreciably higher than on top of the F4TCNQ at bias voltages above 1 V. However, the increase of signal below −0.5 V resembles the feature of surface state localization by adatoms.[37−40] The same but weaker features are also observed on top of the F4TCNQ molecules, suggesting also some LUMO component. Similarly, the double feature in the positive bias range at +0.4 and +0.75 V, tentatively assigned to the LUMO, can contain some Au(111) surface state component shifted upward in energy.[35,42−44] Figure 3b shows a constant current dI/dV map

dx.doi.org/10.1021/jp306780n | J. Phys. Chem. C 2012, 116, 24558−24565

taken at V = +450 mV (right panel) and the corresponding STM topography (left panel). The bright stripes in the dI/dV map correspond to the F4TCNQ rows in the STM topography. Note, that contrary to the STM topography the dI/dV map shows higher signal between the molecules. This effect is produced by the constant current mode measurement (closed feedback loop) where the vertical tip displacement, determined by the STM topography enhances the dI/dV signal at shorter tip−sample distances and vice versa.[41] dI/dV maps taken at different biases within the double peak feature show a similar pattern.

Next, we focus on the Mn−TCNQ system. Figure 4a shows dI/dV spectra taken at the center of the TCNQ molecule (blue curve) and at the Mn adatom position (red curve). There are several significant differences compared to Au−F4TCNQ: (i) the lack of any spectral feature in the dI/dV spectra taken at the center of the TCNQ molecule, (ii) a strong and broad signal that is observed in the range of occupied states in the dI/dV spectrum at the Mn adatom position, and (iii) the absence of any clear spectral feature that can be related to the Au(111) surface state in any of the spectra in a wide bias voltage range from −1 to +1 V. dI/dV spectra of the pure TCNQ adlayer without Mn atoms show a peak at about +0.8 V that can be ascribed to the LUMO of the neutral TCNQ molecule (cf. SI, Figure S3).[35,36] Furthermore, the surface state is still present in the pure molecular layer being shifted up in energy by about 150 mV. Upon coordination with the Mn atoms neither of these two features is observed any more. All together, these observations point toward the existence of a strong hybridization between Au(111) substrate, Mn, and TCNQ states including the quenching of the Au(111) surface state and the mixing between Mn states and the LUMO of the TCNQ molecule. In Figure 4b a dI/dV map taken at V = −450 mV shows high intensity at the Mn and CN groups locations, while the corresponding STM topography at V = −450 mV shows protrusions on top of both the TCNQ molecules and the Mn atoms. These observations are consistent with the dI/dV spectra shown in Figure 4a taking into account the modulation effect in the constant current acquisition mode. (See also Figure S4 in the SI with an STM topography taken at +500 mV showing bright contrast on the TCNQ molecules only.)

To interpret the features observed in the STS data we have calculated the projected density of states (PDOS) onto atomic and molecular orbitals. In particular, we focus on the projections onto the highest occupied molecular orbital (HOMO) and LUMO of the ligand molecules, onto the atomic s and out-of-plane p_z orbitals of the N atom and different C atoms discriminating between the cyano group and the central ring, as well as onto the Au and Mn adatom orbitals. Note that these periodic supercell DFT calculations have limitations. First of all, the phenomenon of surface state localization cannot be reproduced using a finite size surface unit cell slab of only four layers. In addition, DFT does not yield the correct HOMO−LUMO gap (it is underestimated) nor the precise HOMO and LUMO energy location with respect to the Fermi level. However, major trends for the two systems can be discussed.

In Figure 5 the PDOS onto the F4TCNQ molecular states, as well as N and C atom components, is plotted together with the Au adatom DOS. The LUMO is positioned near the Fermi level, while the HOMO is about 1.5 eV lower in energy, consistent with a charge transfer of about one electron to the F4TCNQ acceptor molecule. A Bader analysis gives a total

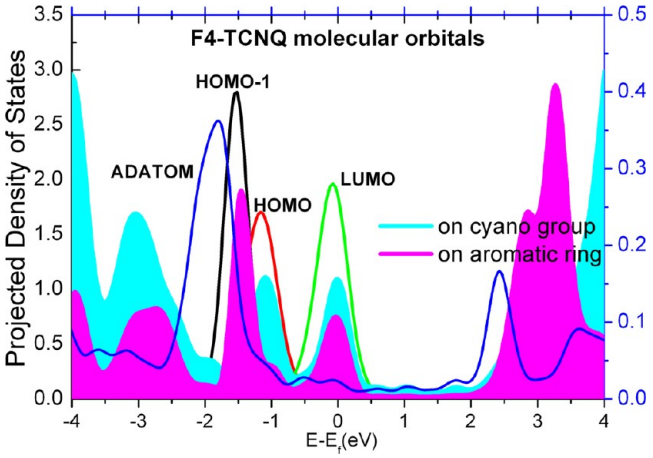

Figure 5. Projected density of states (PDOS) of F4TCNQ/Au(111) onto different molecular and atomic orbitals. Black, red and green lines correspond to the HOMO-1, HOMO and LUMO of F4TCNQ. PDOS onto atomic orbitals (s and p_z) for cyano and aromatic ring groups of F4TCNQ correspond to blue and pink shaded areas, respectively. PDOS onto atomic orbitals (s + p_z + d) of the Au adatom is plotted in the dark blue line with scale at the right vertical axis.

value of 0.9 e$^-$ originating in part from the Au adatom (0.61 e$^-$) and the Au(111) surface (0.29 e$^-$). The analysis of the molecular PDOS shows that the HOMO has larger weight on the ring than the cyano groups in comparison with the LUMO. We are quite confident about this robust DFT result of an extra electron charge in the F4TCNQ, consistent with the calculated LUMO at the Fermi level. However, it is about 0.4 eV below the broad spectral feature observed in the dI/dV spectra. Therefore, our DFT result would be consistent with the formation of two interface states with a strong LUMO and surface state character. These interface states close to the Fermi level would have different occupation, that is, one below (the bonding combination) and the other one above (the antibonding combination). However, the whole picture is not that simple as there is a third partner coming into play: the segregated Au adatom from the pristine Au(111) herringbone reconstruction. Concerning the Au adatom DOS, it does not show any strong features in this energy range, consistent with the absence of dI/dV signal in the conductance map shown in Figure 3b. In other words, no significant hybridization between the LUMO and Au adatom orbitals is observed.

The PDOS analysis for the Mn−TCNQ system is presented in Figure 6. Although it corresponds to a spin polarized DFT +U calculation to account for the Mn magnetic moment (see Methods section), the sum of the two spin components is plotted for comparison with the Au−F4TCNQ system. The calculated value of the Mn atoms magnetic moment in the self-assembled monolayer (4.6 μ_B) is essentially not quenched from its atomic value (5 μ_B) but no significant spin polarization is induced in the TCNQ molecules. Apart from this, there are pronounced differences compared to the Au−F4TCNQ overlayer. The PDOS onto TCNQ molecular orbitals spreads over a wider energy range below the Fermi level. The two peaks around −0.3 eV correspond to the LUMOs of the two TCNQ molecules in the surface unit cell. A Bader analysis yields a charge transfer of 1.5 e$^-$ to the TCNQ LUMO that essentially comes entirely from the Mn atom. The PDOS onto the Mn adatom orbitals also shows a peak at the LUMO position and another contribution at −1.2 eV. The latter peak coincides with

dx.doi.org/10.1021/jp306780n | J. Phys. Chem. C 2012, 116, 24558−24565

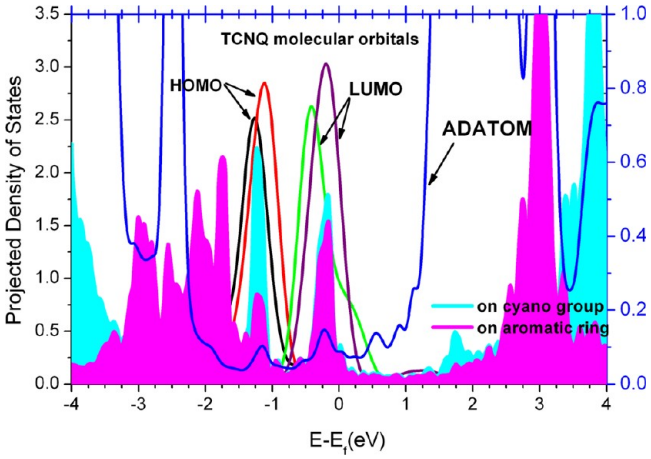

Figure 6. Projected density of states (PDOS) of Mn−TCNQ/Au(111). PDOS onto molecular orbitals of TCNQ are plotted with red and black lines for the HOMO, while green and purple are for the LUMO. The double peaks related to HOMO and LUMO are due to the presence of two TCNQ molecules in the unit cell. PDOS onto atomic orbitals (s and p_z) for cyano and aromatic ring groups correspond to blue and pink shaded areas, respectively. The PDOS onto atomic orbitals (s + p_z + d) of the Mn atom is plotted in the dark blue line with scale at the right vertical axis.

a strong molecular PDOS signal that originates from the CN groups as a high energy HOMO component. Thus, in contrast to Au−F4TCNQ the Mn−TCNQ bonding has some covalent character with significant hybridization between the Mn d-orbitals and the HOMO and LUMO states of TCNQ. The wide energy spread of the PDOS onto TCNQ molecular orbitals is consistent with the lack of spectral features on the ligand molecules, while the spectral weight at −0.3 eV in the PDOS is assigned to the observed broad peak at −0.5 V in the dI/dV spectrum on the Mn atom (cf. Figure 4a). This also explains the signal pattern observed in the dI/dV map with high intensity at the Mn position including the CN groups in its surrounding (see Figure 4b).

CONCLUSIONS

We have demonstrated that metal−organic charge transfer networks exhibiting single Au and Mn centers can be synthesized on a Au(111) surface using strong electron accepting ligand molecules. On the basis of STM data and first principles calculations, we have found that the two structurally similar networks have different electronic properties depending on the type of metal center and its coordination number, both having the same stoichiometry. The coordination of the metal center (Au or Mn) and the type of bond are important in determining the degree of charge transfer to the molecules from the metal centers. However, the rather inert Au(111) surface plays a minor role in the charge transfer process as compared, for example, with the Mn−TCNQ$_2$ metal−organic network on Cu(100), where the TCNQ LUMO becomes doubly occupied on Cu(100) even in the absence of Mn adatoms.[14,25] In the Mn−TCNQ/Au(111) network the charge donation to the TCNQ molecules originates almost exclusively from the Mn atoms and results in an almost fully occupied LUMO. It is only partially occupied for F4TCNQ, despite its much higher electron affinity, and also points toward a major participation (about one-third of the total charge donated to the F4TCNQ) of the Au(111) surface in the charge transfer to the F4TCNQ. Thus, the differences in charge transfer of the two systems reflect the importance of (i) the character of the bond, F4TCNQ-Au or TCNQ-Mn, and (ii) the 4-fold versus 2-fold coordination in Mn−TCNQ as compared to Au−F4TCNQ. This is determined by the different Mn and Au adsorption sites that result from the different N−Au and N−Mn bond lengths. In addition, low-temperature high-resolution tunnelling spectroscopy data suggest that the pristine Au(111) surface state can be either quenched or split and localized at the Mn or Au adatom site, respectively, due to its coupling to the LUMO of the strong acceptor molecules. Finally, we find that the magnetic moment of the Mn metal centers is practically not quenched from the corresponding Mn atom value and, therefore, calls for a thorough investigation of the magnetic properties of two-dimensional metal−organic coordination networks on inert surfaces.

ASSOCIATED CONTENT

Supporting Information

Large scale STM topographical images of the two systems under study are included in Figures S1 and S2. They show the removal of the Au(111) herringbone reconstruction after F4TCNQ adsorption but not with TCNQ and Mn atoms. Figure S3 corresponds to an STM image showing the coexistence of a pure TCNQ phase and the Mn−TCNQ phase, together with the corresponding dI/dV spectra, while Figure S4 shows the change of contrast with bias voltage polarity in STM topographical images of the Mn−TCNQ metal organic coordination network. This information is available free of charge via the Internet at http://pubs.acs.org.

AUTHOR INFORMATION

Corresponding Author

*E-mail: s.stepanow@fkf.mpg.de; andres.arnau@ehu.es.

Author Contributions

#These authors contributed equally to this article.

Notes

The authors declare no competing financial interest.

ACKNOWLEDGMENTS

N.J., S.S., A.L., and K.K. acknowledge support by the Baden-Württemberg Stiftung. M.N.F., N.G-L., and A.A. thank the Spanish Ministerio de Ciencia e Innovación (Grant No. FIS2010-19609-C02-01) and the Basque Government (Grant No. IT-366-07) for financial support.

REFERENCES

(1) Stepanow, S.; Lingenfelder, M.; Dmitriev, A.; Spillmann, H.; Delvigne, E.; Lin, N.; Deng, X.; Cai, Ch.; Barth, J. V.; Kern, K. Steering molecular organization and host−guest interactions using two-dimensional nanoporous coordination systems. *Nat. Mater.* **2004**, *3*, 229.

(2) Barth, J. V.; Constantini, G; Kern, K. Engineering atomic and molecular nanostructures at surfaces. *Nature* **2005**, *437*, 671−679.

(3) Schlickum, U.; Decker, R.; Klappenberger, F.; Zoppellaro, G.; Klyatskaya, S.; Ruben, M.; Silanes, I.; Arnau, A.; Kern, K.; Brune, H.; Barth, J. V. Metal−organic honeycomb nanomeshes with tunable cavity size. *Nano Lett.* **2007**, *7* (12), 3813−3817.

(4) Pawin, G.; Wong, K. L.; Kim, D.; Sun, D.; Bartels, L.; Hong, S.; Rahman, T. S.; Carp, R.; Marsella, M. A surface coordination network based on substrate−derived metal adatoms with local charge excess. *Angew. Chem., Int. Ed.* **2008**, *47*, 8442.

(5) Henningsen, N.; Rurali, R.; Limbach, C.; Drost, R.; Pascual, J. I.; Franke, K. J. Site-dependent coordination bonding in self-assembled metal−organic networks. *J. Phys. Chem. Lett.* **2011**, *2*, 55−61.
(6) Gambardella, P.; Stepanow, S.; Dmitriev, A.; Honolka, J.; de Groot, F. M. F.; Lingenfelder, M.; Gupta, S. S.; Sarma, D. D.; Bencok, P.; Stanescu, S.; et al. Supramolecular control of the magnetic anisotropy in two-dimensional high-spin Fe arrays at a metal interface. *Nat. Mater.* **2009**, *8*, 189.
(7) Fabris, S.; Stepanow, S.; Lin, N.; Gambardella, P.; Dmitriev, A.; Honolka, J.; Baroni, S.; Kern, K. Oxygen dissociation by concerted action of di-iron centers in metal−organic coordination networks at surfacecs: Modeling non-heme iron enzymes. *Nano Lett.* **2011**, *11*, 5414.
(8) Decker, R.; Schlickum, U.; Klappenberger, F.; Zoppellaro, G.; Klyatskaya, S.; Ruben, M.; Barth, J. V.; Brune, H. Using metal−organic templates to steer the growth of Fe and Co nanoclusters. *Appl. Phys. Lett.* **2008**, *93*, 243102.
(9) Li, Y.; Xiao, J.; Shubina, T. E.; Chen, M.; Shi, Z.; Schmid, M.; Steinrück, H.-P.; Gottfried, J. M.; Lin, N. Coordination and metalation bifunctionality of Cu with 5,10,15,20-tetra(4-pyridyl)porphyrin: Toward a mixed-valence two-dimensional coordination network. *J. Am. Chem. Soc.* **2012**, *134*, 6401.
(10) Walch, H.; Dienstmaier, J.; Eder, G.; Gutzler, R.; Schlögl, S.; Sirtl, T.; Das, K.; Schmittel, M.; Lackinger, M. Extended two-dimensional metal−organic frameworks based on thiolate-copper coordination bonds. *J. Am. Chem. Soc.* **2011**, *133*, 7909.
(11) Tait, S. L.; Langner, A.; Lin, N.; Stepanow, S.; Rajadurai, Ch.; Ruben, M.; Kern, K. One-dimensional self-assembled molecular chains on Cu(100): Interplay between surface-assisted coordination chemistry and substrate commensurability. *J. Phys. Chem. C* **2007**, *111*, 10982−10987.
(12) Bedwani, S.; Wegner, D.; Crommie, M. F.; Rochefort, A. Strongly reshaped organic−metal interfaces: Tetracyanoethylene on Cu(100). *Phys. Rev. Lett.* **2008**, *101*, 216105−216108.
(13) Bjork, J.; Matena, M.; Dyer, M. S.; Enache, M.; Lobo-Checa, J.; Gade, L. H.; Jung, T. A.; Stohr, M.; Persson, M. STM fingerprint of molecule-adatom interactions in a self-assembled metal−organic surface coordination network on Cu(111). *Phys. Chem. Chem. Phys.* **2010**, *12*, 8815−8821.
(14) Tseng, T.-C.; Urban, C.; Wang, Y.; Otero, R.; Tait, S. L.; Alcami, M.; Ecija, D.; Trelka, M.; Gallego, J. M.; Lin, N.; et al. Charge-transfer-induced structural rearrangements at both sides of organic metal interfaces. *Nat. Chem.* **2010**, *2*, 374−379.
(15) Baber, A. E.; Jensen, S. C.; Iski, E. V.; Sykes, E. C. H. Extraordinary atomic mobility of Au111 at 80 K: Effect of styrene adsorption. *J. Am. Chem. Soc.* **2006**, *128*, 15384−15385.
(16) Driver, S. M.; Zhang, T.; King, D. A. Massively cooperative adsorbate-induced surface restructuring and nanocluster formation. *Angew. Chem., Int. Ed.* **2007**, *46*, 700−703.
(17) Rossel, F; Brodard, P.; Patthey, F.; Richardson, N. V.; Schneider, W.-D. Modified herringbone reconstruction on Au(111) induced by self-assembled Azure A islands. *Surf. Sci.* **2008**, *602*, L115−L117.
(18) Voznyy, O.; Dubowski, J. J.; Yates, J. T., Jr.; Maksymovych, P. The role of gold adatoms and stereochemistry in self-assembly of methylthiolate on Au(111). *J. Am. Chem. Soc.* **2009**, *131*, 12989−12993.
(19) Pan, Y.; Yang, B.; Hulot, C.; Blechert, S.; Nilius, N.; Freund, H. J. Effect of lattice-gas atoms on the adsorption behaviour of thioether molecules. *Phys. Chem. Chem. Phys.* **2012**, *14*, 10987−10993.
(20) Lazarovits, B.; Szunyogh, L.; Weinberger, P. Spin-polarized surface states close to adatoms on Cu(111). *Phys. Rev. B* **2006**, *73*, 045430.
(21) Abdurakhmanova, N.; Floris, A.; Tseng, T.-C.; Comisso, A.; Stepanow, S.; De Vita, A.; Kern., K. Stereoselectivity and electrostatics in charge-transfer Mn− and Cs−$TCNQ_4$ networks on Ag(100). *Nat. Commun.* **2012**, *3*, 940.
(22) Koch, N.; Duhm, S.; Rabe, J. P. Optimized hole injection with strong electron acceptors at organic-metal interfaces. *Phys. Rev. Lett.* **2005**, *95*, 237601.
(23) Romaner, L.; Heimel, G.; Bredas, J. L.; Gerlach, A.; Schreiber, F.; Johnson, R. L.; Zegenhagen, J.; Duhm, S.; Koch, N.; Zojer, E. Impact of bidirectional charge transfer and molecular distortions on the electronic structure of a metal−organic interface. *Phys. Rev. Lett.* **2007**, *99*, 256801.
(24) Jaeckel, F.; Perea, U. G. E.; Iancu, V.; Braun, K.-F.; Koch, N.; Rabe, J. P.; Hla, S. W. Investigating molecular charge transfer complexes with a low temperature scanning tunneling microscope. *Phys. Rev. Lett.* **2008**, *100*, 126102.
(25) Tseng, T.-C.; Lin, Ch.; Shi, X.; Tait, S. L.; Liu, X.; Starke, U.; Lin, N.; Zhang, R.; Minot, Ch.; Van Hove, M. A.; et al. Two-dimensional metal−organic coordination networks of Mn-7,7,8,8-tetracyanoquinodimethane assembled on Cu(100): Structural, electronic, and magnetic properties. *Phys. Rev. B* **2009**, *80*, 155458.
(26) Tseng, T.-C.; Abdurakhmanova, N.; Stepanow, S.; Kern, K. Hierarchical assembly and reticulation of two-dimensional Mn and Ni $TCNQ_x$ (x = 1,2,4) coordination structures on a metal surface. *J. Phys. Chem C* **2011**, *115*, 10211.
(27) Kresse, G.; Hafner, J. Ab initio molecular-dynamics simulation of the liquid−metal−amorphous−semiconductor transition in germanium. *Phys. Rev. B* **1994**, *49*, 14251−14269.
(28) Kresse, G.; Furthmuller, J. Efficient iterative schemes for ab initio total-energy calculations using a plane-wave basis set. *Phys. Rev. B* **1996**, *54*, 11169−11186.
(29) Bloch, P. E. Projector augmented-wave method. *Phys. Rev. B* **1994**, *50*, 17953−17979.
(30) Perdew, J. P.; Chevary, J. A.; Vosko, S. H.; Jackson, K. A.; Pederson, M. R.; Singh, D. J.; Fiolhais, C. Atoms, molecules, solids, and surfaces: Applications of the generalized gradient approximation for exchange and correlation. *Phys. Rev. B* **1992**, *46*, 6671−6687.
(31) Dudarev, S. L.; Boton, G. A.; Savrasov, S. Y.; Humphreys, C. J.; Sutton, A. P. Electron-energy-loss spectra and the structural stability of nickel oxide: An LSDA+U study. *Phys. Rev. B* **1998**, *57*, 1505−1509.
(32) Tersoff, J.; Hamann, D. R. Theory of the scanning tunneling microscope. *Phys. Rev. B* **1985**, *31*, 805−813.
(33) Mina, B. K.; Alemozafara, A. R.; Bienera, M. M.; Bienera, J.; Friend, C. M. Reaction of Au(111) with sulfur and oxygen: Scanning tunneling microscopic study. *Top. Catal.* **2005**, *36*, 77−90.
(34) Gao, W.; Baker, T. A.; Zhou, L.; Pinnaduwage, D. S.; Kaxiras, E.; Friend, C. M. Chlorine adsorption on Au(111): Chlorine overlayer or surface chloride? *J. Am. Chem. Soc.* **2008**, *130*, 3560−3565.
(35) Gonzalez-Lakunza, N.; Fernandez-Torrente, I.; Franke, K. F.; Lorente, N.; Arnau, A.; Pascual, J. I. Formation of dispersive hybrid bands at an organic−metal interface. *Phys. Rev. Lett.* **2008**, *100*, 156805.
(36) Fernandez Torrente, I.; Franke, K. J.; Pascual, J. I. Structure and electronic configuration of tetracyanoquinodimethane layers on a Au(111) surface. *Int. J. Mass Spectrom.* **2008**, 277.
(37) Olsson, F. E.; Persson, M; Borisov, A. G.; Gauyacq, J.-P.; Lagoute, J.; Folsch, S. Localization of the Cu(111) surface state by single Cu adatoms. *Phys. Rev. Lett.* **2004**, *93*, 206803.
(38) Limot, L.; Pehlke, E.; Kröger, J.; Berndt, R. Surface-state localization at adatoms. *Phys. Rev. Lett.* **2005**, *94*, 036805.
(39) Stepanyuk, V. S.; Klavsyuk, A. N.; Niebergall, L.; Bruno, P. End electronic states in Cu chains on Cu(111): Ab initio calculations. *Phys. Rev. B* **2005**, *72*, 153407.
(40) Schouteden, K.; Lievens, P.; Van Haesendonck, C. Low-temperature STM/STS investigation of nanostructures created by an STM tip on Au(111) surfaces. *Appl. Phys. A: Mater. Sci. Process.* **2009**, *96*, 409−413.
(41) Ziegler, M.; Néel, N.; Sperl, A.; Kröger, J.; Berndt, R. Local density of states from constant−current tunneling spectra. *Phys. Rev. B* **2009**, *80*, 125402.
(42) Temirov, R.; Soubatch, S.; Luican, A.; Tautz, F. S. Free-electron-like dispersion in an organic monolayer film on a metal substrate. *Nature* **2006**, *444*, 350.
(43) Schwalb, C. H.; Sachs, S.; Marks, M.; Schöll, A.; Reinert, F.; Umbach, E. Höfer Electron lifetime in a Shockley-type metal−organic interface state. *Phys. Rev. Lett.* **2008**, *101*, 146801.

(44) Zaitsev, N. L.; Nechaev, I. A.; Echenique, P. M.; Chulkov, E. V. Transformation of the Ag(111) surface state due to molecule−surface interaction with ordered organic molecular monolayers. *Phys. Rev. B* **2012**, *85*, 115301.
(45) Shi, X. C.; Lin, C.; Minot, C.; Tseng, T. C.; Tait, S. L.; Lin, N.; Zhang, R. Q.; Kern, K.; Cerda, J. I.; Van Hove, M. A. Structural analysis and electronic properties of negatively charged TCNQ: 2D networks of $(TCNQ)_2Mn$ assembled on Cu(100). *J. Phys. Chem. C* **2010**, *114*, 17197.